



Cite this: *RSC Adv.*, 2019, 9, 21660

# Systematic study of TiO<sub>2</sub>/ZnO mixed metal oxides for CO<sub>2</sub> photoreduction†

Warren A. Thompson,<sup>†</sup> Alberto Olivo,<sup>‡</sup> Danny Zanardo,<sup>‡</sup> Giuseppe Cruciani,<sup>d</sup> Federica Menegazzo,<sup>c</sup> Michela Signoretto,<sup>ib</sup> and M. Mercedes Maroto-Valer<sup>a</sup>

A two component three degree simplex lattice experimental design was employed to evaluate the impact of different mixing fractions of TiO<sub>2</sub> and ZnO on an ordered mesoporous SBA-15 support for CO<sub>2</sub> photoreduction. It was anticipated that the combined advantages of TiO<sub>2</sub> and ZnO: low cost, non-toxicity and combined electronic properties would facilitate CO<sub>2</sub> photoreduction. The fraction of ZnO had a statistically dominant impact on maximum CO<sub>2</sub> adsorption ( $\beta_2 = 22.65$ ,  $p$ -value =  $1.39 \times 10^{-4}$ ). The fraction of TiO<sub>2</sub> used had a statistically significant positive impact on CO ( $\beta_1 = 9.71$ ,  $p$ -value =  $2.93 \times 10^{-4}$ ) and CH<sub>4</sub> ( $\beta_1 = 1.43$ ,  $p$ -value =  $1.35 \times 10^{-3}$ ) cumulative production. A negative impact, from the interaction term between the fractions of TiO<sub>2</sub> and ZnO, was found for CH<sub>4</sub> cumulative production ( $\beta_3 = -2.64$ ,  $p$ -value =  $2.30 \times 10^{-2}$ ). The systematic study provided evidence for the possible loss in CO<sub>2</sub> photoreduction activity from sulphate groups introduced during the synthesis of ZnO. The decrease in activity is attributed to the presence of sulphate species in the ZnO prepared, which may possibly act as charge carrier and/or radical intermediate scavengers.

Received 7th May 2019  
Accepted 1st July 2019

DOI: 10.1039/c9ra03435h

rsc.li/rsc-advances

## 1 Introduction

CO<sub>2</sub> photoreduction is one of the potential technologies for carbon utilisation.<sup>1</sup> However, major optimization in photocatalyst design is required for its applicability.<sup>2</sup> Possible approaches in heterogeneous photocatalysis to improve photocatalytic activity include photocatalyst dispersion on highly porous substrates and the use of coupling two semiconductors as photocatalysts. For these reasons, composite mixtures of ZnO and TiO<sub>2</sub> were prepared on an ordered mesoporous SBA-15 silica support for CO<sub>2</sub> photoreduction. SBA-15 was chosen as it has several favourable characteristics including: a large surface area which may enhance photocatalyst dispersion and the availability of photons;<sup>3</sup> SBA-15 is also chemically and mechanically stable<sup>4</sup> and SBA-15 has shown effectiveness as a CO<sub>2</sub> photoreduction support.<sup>5-7</sup>

TiO<sub>2</sub> has been shown to be an effective photocatalyst for CO<sub>2</sub> photoreduction with numerous examples found in the literature.<sup>1,8,9</sup> ZnO has also shown promise as a photocatalyst for CO<sub>2</sub>

photoreduction.<sup>10-12</sup> ZnO offers improved CO<sub>2</sub> adsorption<sup>12</sup> and low charge carrier recombination.<sup>13</sup> Both TiO<sub>2</sub> and ZnO share low cost, non-toxicity and relatively environmentally friendly properties.<sup>1,14</sup>

TiO<sub>2</sub> is not efficient for CO<sub>2</sub> photoreduction due to: poor charge carrier mobility leading to a fast recombination rate<sup>13</sup> and hindered CO<sub>2</sub> adsorption in the presence of H<sub>2</sub>O due to the limited presence of surface basic functionalities.<sup>15</sup> On the contrary, ZnO exhibits a longer charge carrier lifetime<sup>16</sup> and suitable surface basicity,<sup>17</sup> which can improve CO<sub>2</sub> adsorption. Moreover, the coupling of TiO<sub>2</sub> and ZnO, was reported to form a heterojunction that could reduce charge carrier recombination leading to enhanced CO<sub>2</sub> photoreduction activity.<sup>18</sup> Composite mixtures of anatase TiO<sub>2</sub> and wurtzite-type ZnO, due to the TiO<sub>2</sub>/ZnO heterojunction formed, showed improved CO<sub>2</sub> photoreduction activity.<sup>19</sup> Other examples of composite mixtures of TiO<sub>2</sub> and ZnO leading to improved photocatalytic activity, due to less charge recombination, include the degradation of phenols and salicylic acid.<sup>20,21</sup> Due to their synergistic effects on electronic and acid/base properties, the use of TiO<sub>2</sub> and ZnO as photocatalyst mixture is promising for CO<sub>2</sub> photoreduction. However, no examples have described the impact of different mixing fractions of TiO<sub>2</sub> and ZnO on CO<sub>2</sub> photoreduction performance.

CO<sub>2</sub> photoreduction faces the challenge of low efficiency but also the deactivation of the photocatalyst.<sup>22</sup> Deactivation of the photocatalyst has been reported, especially when production data is collected in continuous flow setups, for CO<sub>2</sub> photoreduction by a growing number of authors.<sup>23-32</sup> Possible

<sup>a</sup>Research Centre for Carbon Solutions (RCCS), School of Engineering & Physical Sciences, HeriotWatt University, Edinburgh, EH14 4AS, UK. E-mail: wat1@hw.ac.uk

<sup>b</sup>Low Emission Resources Corporation, 2 Mid Craigie Rd, Dundee, DD4 7RH, UK

<sup>c</sup>CatMat Lab, Dept. of Molecular Sciences and Nanosystems, Ca' Foscari University Venice, Consortium INSTM, RU of Venice, Via Torino 155, 30172 Venezia, Italy

<sup>d</sup>Department of Physics and Earth Sciences, University of Ferrara, Via G. Saragat 1, Ferrara, I-44122, Italy

† Electronic supplementary information (ESI) available. See DOI: 10.1039/c9ra03435h

‡ These authors contributed equally to this work.



explanations for deactivation include: photocatalyst poisoning due to irreversible adsorption of reaction intermediates; sintering and agglomeration of the photocatalyst metal active sites and loss of active reaction sites that include oxygen vacancies, surface hydroxyls and  $\text{Ti}^{3+}$  sites.<sup>22</sup> To develop  $\text{CO}_2$  photoreduction, low efficiency and deactivation of the photocatalyst need to be addressed. In a closely related field of photocatalytic oxidation, radical scavenging of the reactive oxygen species as hydroxyl radicals have been found to lead to deactivation.<sup>33</sup> Some inorganic anions are known to interact with radical processes, by yielding less reactive and more stable intermediates and thus hampering the overall photocatalytic reaction.<sup>34</sup>

High throughput technologies and automation are critical to finding suitable photocatalysts.<sup>35</sup> Central to these technologies is the use of systematic experimental designs, Design of Experiments (DOE), for decision making. There are numerous examples in the literature describing the use of DOE for engineering and process optimisation.<sup>29,36,37</sup> Mixture designs can efficiently evaluate the impact of component fractions in a mixture.<sup>38</sup> In this work, the impact of  $\text{TiO}_2$  and  $\text{ZnO}$  fractions used for the formulation of a mixed metal oxide (MO) photocatalyst mixture on a SBA-15 support, was evaluated for  $\text{CO}_2$  photoreduction using a novel combination of a systematic mixture design and photocatalysis theory.

In this work in-house synthesis of the photocatalysts was used due to the potential and scope, using different synthetic methodologies, for improvements to increase surface area, crystallinity,<sup>39</sup> photocatalyst coverage and optical properties.<sup>29</sup>

## 2 Experimental

### 2.1 Photocatalyst preparation

SBA-15 was synthesized according the procedure reported in literature.<sup>40</sup> Briefly, template EO20-PO70-EO20 (P123, Aldrich) was dissolved in aqueous HCl solution and tetraorthosilicate (TEOS) was introduced as silica precursors. Powder was aged at 90 °C, dried and then calcined at 550 °C for 6 h under air flow.  $\text{TiO}_2$  and  $\text{ZnO}$  were synthesised by precipitation of inorganic salts. In the case of  $\text{TiO}_2$ , a titanyl sulphate solution and a NaOH solution were added dropwise to deionised  $\text{H}_2\text{O}$  under vigorous stirring, keeping pH neutral. Then the  $\text{Ti}(\text{OH})_4$  suspension was aged at 60 °C for 20 h and then washed with distilled  $\text{H}_2\text{O}$  to remove the sulphate ions and dried at 110 °C for 18 h and finally calcined at 400 °C for 4 h in air flow.<sup>41</sup>  $\text{ZnO}$  was prepared following the same procedure reported for  $\text{TiO}_2$ , but starting from a  $\text{ZnSO}_4$  solution as precursor and keeping the pH slightly alkaline (pH 9) during the precipitation. The prepared  $\text{TiO}_2$  and  $\text{ZnO}$  were added onto SBA-15 by incipient wetness impregnation using isopropanol as a liquid medium. Samples were then dried at 110 °C for 18 h.

### 2.2 UV-vis absorption

The light absorption and electronic band were characterized using a UV-vis spectrometer (PerkinElmer lamda 950) equipped with a 150 mm integration sphere (PerkinElmer). The band gap

was determined using the Kubelka–Munk function (1) and intersection of the Tauc segment and  $h\nu$ -axis of the Tauc plot.<sup>42</sup>

$$F(R_\infty) = \frac{(1 - R_\infty^2)}{2R_\infty} \quad (1)$$

where  $F(R_\infty)$  is the reemission function and  $R_\infty$  is the reflectance of the sample with infinite thickness.

### 2.3 XRD characterisation

For the analysis of mixed MOs on SBA-15, a Bruker D8 Advance powder diffractometer, operating with Ge-monochromated  $\text{Cu K}\alpha$  radiation (wavelength = 1.5406 Å) and a LynxEye linear detector. Data were collected over the angular range 5–85° in  $2\theta$ . For the analysis of pure  $\text{ZnO}$  and  $\text{TiO}_2$ , X-ray Diffraction (XRD) patterns were collected on a Bruker D8 Advance powder diffractometer with a sealed X-ray tube (copper anode, 40 kV and 40 mA) and a Si(Li) solid state detector (Sol-X) set to discriminate the  $\text{Cu K}\alpha$  radiation. Apertures of divergence, receiving, and detector slits were 2.0 mm, 2.0 mm, and 0.2 mm, respectively. Data scans were performed in the  $2\theta$  range 5–75° with 0.02° step size and counting times of 3 s per step. Quantitative phase analysis determination performed using the Rietveld method as implemented in the TOPAS v.4 program (Bruker AXS) using the fundamental parameters approach for line-profile fitting.

### 2.4 $\text{N}_2$ physisorption

Specific surface areas (SSA) of the samples were evaluated by  $\text{N}_2$  physisorption. 200 mg of the sample was placed under vacuum at 200 °C for 2 h. The analyses were then carried out recording the adsorption–desorption isotherm at –196 °C with a Micromeritics ASAP 2000 analyzer. SSAs were finally determined by the BET equation.<sup>43</sup>

### 2.5 $\text{CO}_2$ adsorption

Samples were degassed under a constant purge of  $\text{N}_2$  at 200 °C for 10 h.  $\text{CO}_2$  adsorption capacities were estimated by the maximum value found from the  $\text{CO}_2$  adsorption isotherm measured at 273 K over fifteen equidistant points from 0 to 0.95  $P/P_0$  (Gemini VII 2390).

### 2.6 $\text{CO}_2$ photoreduction tests

A slurry of the prepared mixed MO photocatalyst was prepared by adding  $\approx 100$  mg of the mixed MO photocatalyst to 1 ml DI  $\text{H}_2\text{O}$  in a 5 ml vial. The vial was sealed and agitated in an ultrasonic bath for two minutes. The slurry was then deposited dropwise onto a glass fiber disc (47 mm diameter). The coated glass fiber disc was dried at 120 °C for 2 h. The coated glass fiber disc was placed in the middle of a stainless steel photoreactor ( $r = 25$  mm,  $h = 1$  mm,  $v = 1.96$  mm<sup>3</sup>) and sealed. Residual air in the system was evacuated *via* three repetitive steps of placing the system under vacuum to –1 bar and the vacuum released with  $\text{CO}_2$  (99.995%) to +1 bar. The flow rate of  $\text{CO}_2$  was set to 0.35 ml min<sup>–1</sup> and passed through the temperature controlled ( $\pm 0.1$  °C) aluminium body saturator for at least 12 h to allow the



system to equilibrate. Relative humidity ( $\pm 1.8\%$  RH) was measured using an inline Sensirion SHT75 humidity sensor potted (MG Chemicals 832HD) into a Swagelok 1/4" T-piece. The temperature of the photocatalyst surface ( $40\text{ }^\circ\text{C} \pm 2.0\text{ }^\circ\text{C}$ ) was controlled using a hotplate and the surface temperature measured using a Radley's pyrometer. To prevent condensation at higher saturation temperatures, the lines from the outlet of the saturator up until the inlet of the H<sub>2</sub>O trap were heated and temperature controlled ( $\pm 0.1\text{ }^\circ\text{C}$ ) with a heating rope and thermocouple (Fig. 1).

An OmniCure S2000 fitted with a 365 nm filter was used as the light source and the irradiance ( $295.71 \pm 1.60\text{ mW cm}^{-2}$ ) checked before each experiment using an OmniCure R2000 radiometer ( $\pm 5\%$ ). An inline GC (Agilent, Model 7890B series) with a Hayesep Q column (1.5 m), (1/16 inch od, 1 mm id), MolSieve 13 $\times$  (1.2 m), (1/16 inch od, 1 mm id), thermal conductivity detector (TCD), nickel catalysed methanizer and flame ionization detector (FID) was used to analyze the output of the photoreactor every four minutes. CO and CH<sub>4</sub> production rates were recorded in units of  $\mu\text{mol g}_{\text{cat}}^{-1}\text{ h}^{-1}$  using only the mass of active mixed MO photocatalyst/s used with the exclusion of the SBA-15 support mass. Cumulative production ( $\mu\text{mol g}_{\text{cat}}^{-1}$ ) was calculated by integrating the area under the production rate ( $\mu\text{mol g}_{\text{cat}}^{-1}\text{ h}^{-1}$ ) vs. time (h) curve.

## 2.7 Ionic chromatography method for testing sulphates

Quantitative analysis of sulphates was performed through a procedure previously reported for sulphate-doped zirconia.<sup>44</sup> 200 mg of the sample was treated with 250 mL of 0.1 M NaOH solution to extract the sulphates. The suspension was filtered and analyzed. A LC20 ionic chromatographer equipped with a 25  $\mu\text{L}$  injection loop, a AS14 separation column, a AG14 guard column, an acid resin suppressor and a ED40 conductivity detector was used. A buffer solution of 10 mM Na<sub>2</sub>CO<sub>3</sub> and 3.5 mM NaHCO<sub>3</sub> in Milli-Q H<sub>2</sub>O, at room temperature was used as eluent. A calibration curve for quantitative analysis was obtained using standard Na<sub>2</sub>SO<sub>4</sub> solution between 1 and 8 ppm.

## 2.8 SEM/EDX analysis

Scanning electron microscopy and X-ray energy dispersive spectroscopy analysis of the mixed MOs and SBA support were performed using a FEI Scios SEM equipped with an EDAX Octane Plus EDS detector.

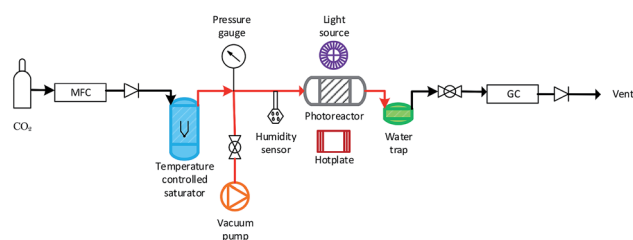


Fig. 1 Overview of the experimental setup used for the MO photocatalyst mixture CO<sub>2</sub> photoreduction tests (not to scale). Pipe lines in red were heated with a temperature controlled heating rope.

Table 1 Two component three degree simplex lattice design points used for experimental settings ( $X_1$  and  $X_2$ ) as mass fractions of TiO<sub>2</sub> and ZnO respectively. Amounts of TiO<sub>2</sub> and ZnO mixed with 800.0 mg SBA-15

Exp. name	$X_1$ fraction TiO <sub>2</sub>	$X_2$ fraction ZnO	Amount TiO <sub>2</sub> (mg)	Amount ZnO (mg)
MO1	1.00	0.00	200.2	0.0
MO2	0.67	0.33	133.9	67.4
MO3	0.33	0.67	66.5	133.2
MO4	0.00	1.00	0.0	200.4
MO5	0.50	0.50	100.4	102.7
MO6	0.75	0.25	149.5	53.5
MO7	0.25	0.75	50.7	150.7

## 2.9 Design of experiments

A two component three degree simplex lattice design was employed with experimental settings and results shown in Table 1. MATLAB was used to estimate: the fitted coefficient values; determine the  $p$ -values and plot the models and data.

The experimental design results were used to fit the polynomial function shown by (2).

$$Y = \beta_1 X_1 + \beta_2 X_2 + \beta_3 X_1 X_2 \quad (2)$$

where  $Y$  is the cumulative production of CO or CH<sub>4</sub>;  $X_1$  and  $X_2$  are the fractions of TiO<sub>2</sub> and ZnO respectively;  $\beta_1$  and  $\beta_2$  are the coefficients estimated for the impact of the fractions of TiO<sub>2</sub> and ZnO used respectively and  $\beta_3$  is the coefficient estimated for the interaction term between the fraction of TiO<sub>2</sub> and ZnO.

Using the matrix of  $X_1$  and  $X_2$  fractions of TiO<sub>2</sub> and ZnO values shown in Table 1 and either the maximum CO<sub>2</sub> adsorption, cumulative production of CO or CH<sub>4</sub> production as a response shown by  $Y$  in (2), the coefficients  $\beta_1$ ,  $\beta_2$  and  $\beta_3$  from (2), were estimated by linear regression using a QR decomposition algorithm (*fitlm* function) in MATLAB (Table 3). The  $p$ -values for each coefficient were determined using the MATLAB *fitlm* function call. Using 95% confidence,  $p$ -values less than 0.05 indicated that the coefficient value was not equal to zero and it's associated parameter ( $X_1$ ,  $X_2$  or  $X_3$ ) had a statistically significant impact on either maximum CO<sub>2</sub> adsorption, CO or CH<sub>4</sub> cumulative production.

# 3 Results and discussion

## 3.1 Characterization and properties of mixed metal oxides

The samples prepared with a high fraction of TiO<sub>2</sub> (MO1, MO2, MO5 and MO6) showed the characteristic broad adsorption peak of anatase TiO<sub>2</sub> (Fig. 2a). As the fraction of ZnO increased (MO3, MO4 and MO7) the Tauc plot peak shapes became sharper and characteristic of the adsorption peaks of ZnO (Fig. 2a). Increasing the fraction of TiO<sub>2</sub> increased the band gap linearly from the ZnO region (3.16 eV) towards the anatase region (3.24 eV) (Fig. 2b).

Decreasing the fraction of TiO<sub>2</sub> reduced the intensity of the characteristic anatase XRD peak (JCPDS Card no. 21-1272) at  $2\theta = 25.4$  (Fig. 3).<sup>45</sup> Increasing the fraction of ZnO increased the



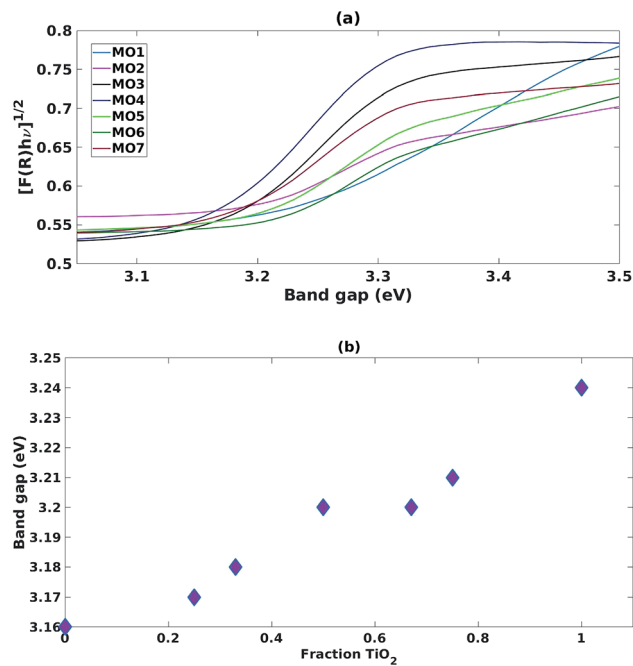


Fig. 2 (a) Tauc plots for mixed MO photocatalysts (b) impact of increasing fraction of  $\text{TiO}_2$  on band gap.

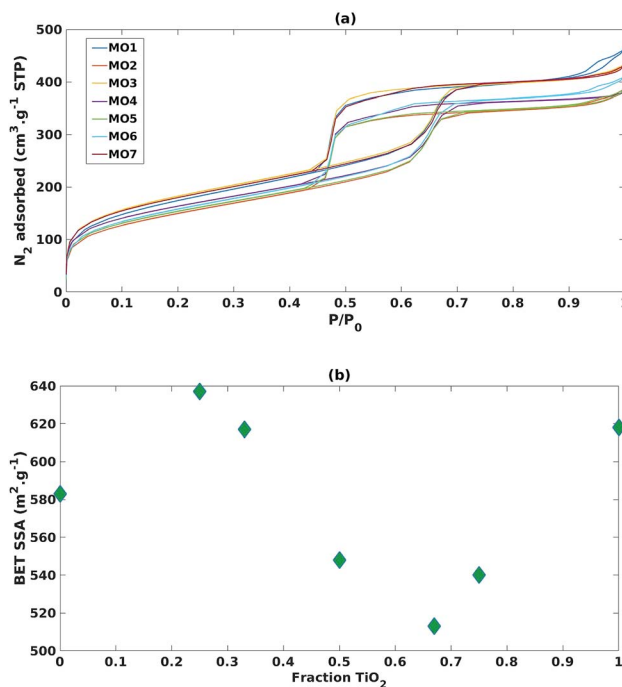


Fig. 4 (a)  $\text{N}_2$  adsorption isotherms of the mixed MO photocatalysts (b) impact of increasing fraction of  $\text{TiO}_2$  on BET specific surface area.

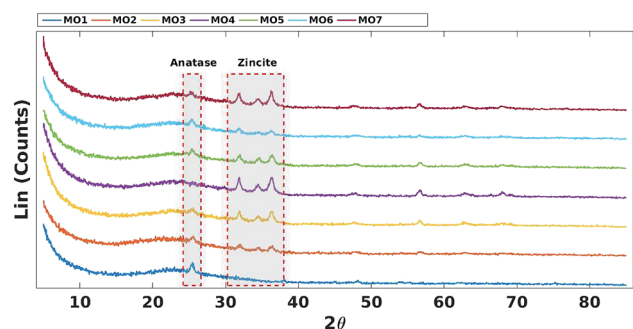


Fig. 3 XRD comparison of mixed MO photocatalysts on SBA-15 support.

intensity of the characteristic zincite peaks (JCPDS card no. 36-1451) at  $2\theta = 31.9, 34.4$  and  $36.2$  (Fig. 3).<sup>46</sup>

As reported in Fig. 4a, adsorption isotherms of all the mixed MO samples exhibited the typical shape of SBA-15, suggesting that its ordered mesoporous structure was retained.<sup>40</sup> Nevertheless, when comparing the SSAs with the  $\text{TiO}_2$  fraction (Fig. 4b), a sinusoidal trend was observed, suggesting that SSA has no or little effect on photoreduction efficiency and selectivity in these mixed MO systems.

### 3.2 Mixture design and the impact of $\text{TiO}_2$ and $\text{ZnO}$ fractions

#### 3.2.1 Impact $\text{TiO}_2$ and $\text{ZnO}$ fractions on $\text{CO}_2$ adsorption.

Fig. 5 shows the impact of increasing the fraction of  $\text{TiO}_2$  used in the mixture on maximum  $\text{CO}_2$  adsorption.  $\text{CO}_2$  adsorption increased significantly when a small fraction of  $\text{ZnO}$  was

present with little change with increasing the fraction of  $\text{ZnO}$  thereafter (Fig. 5).

Both the fraction of  $\text{ZnO}$  and  $\text{TiO}_2$  positively impacted ( $\beta_1 = 19.31$ ,  $\beta_2 = 22.65$ ) maximum  $\text{CO}_2$  adsorption with statistical significance ( $p$ -value =  $2.61 \times 10^{-4}$ ,  $p$ -value =  $1.39 \times 10^{-4}$ ), respectively (Table 2). The impact of the  $\text{ZnO}$  fraction had a larger coefficient value ( $\beta_2 = 22.65$ ) versus  $\text{TiO}_2$  ( $\beta_1 = 19.31$ ) and this could be explained by the increase in surface basicity.<sup>17</sup> It was expected that an increase in  $\text{CO}_2$  adsorption would increase  $\text{CO}_2$  photoreduction photocatalytic activity. However, photocatalytic processes are complicated and often multiple properties of the photocatalyst need to be considered.<sup>1</sup>

**3.2.2 Impact  $\text{TiO}_2$  and  $\text{ZnO}$  fractions on  $\text{CO}_2$  photoreduction.** Fig. 6a and b shows the impact of increasing the fraction of  $\text{TiO}_2$  used in the mixture on  $\text{CO}$  and  $\text{CH}_4$  production, respectively. Increasing the fraction of  $\text{TiO}_2$  increased  $\text{CO}$  cumulative

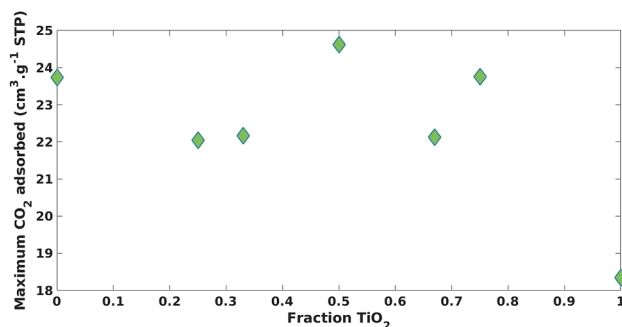
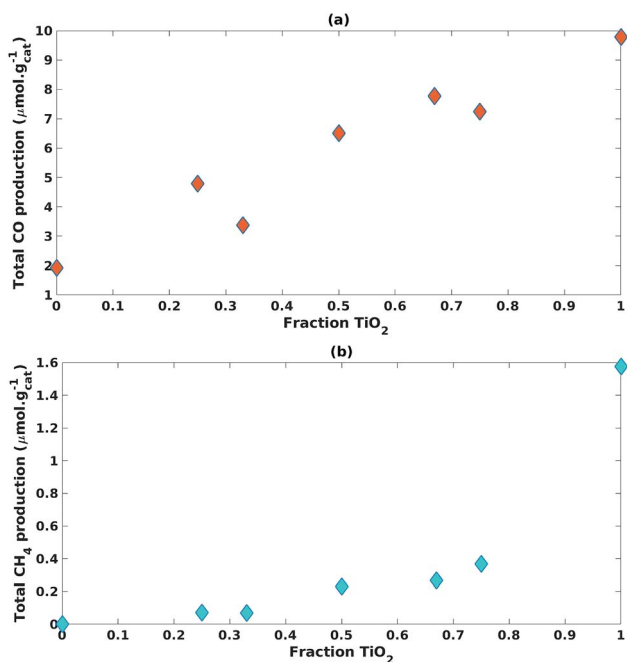


Fig. 5 Impact of increasing fraction of  $\text{TiO}_2$  on of maximum  $\text{CO}_2$  adsorption.



**Table 2** Coefficient values estimated for fitting model (2) and their respective  $p$ -values ( $*p$ -value  $< 0.05$ ) on maximum CO<sub>2</sub> adsorption

Regression results for maximum CO <sub>2</sub> adsorption		
Parameter coefficient	Value estimated	$p$ -Value
$\beta_1$	19.31	$2.61 \times 10^{-4}$ *
$\beta_2$	22.65	$1.39 \times 10^{-4}$ *
$\beta_3$	9.28	$2.32 \times 10^{-1}$



**Fig. 6** Impact of increasing fraction of TiO<sub>2</sub> on (a) CO cumulative production and (b) CH<sub>4</sub> cumulative production.

production with a slight curvature that closely resembled a linear trend (Fig. 6a). Eliminating ZnO from the photocatalyst mixture yielded a significant increase in CH<sub>4</sub> cumulative production with a trend resembling an exponential curve (Fig. 6b).

The TiO<sub>2</sub> fraction in the photocatalyst mixture positively impacted ( $\beta_1 = 9.71$ ) CO cumulative production with statistical significance ( $p$ -value =  $2.93 \times 10^{-4}$ ) (Table 3). This was also the case for CH<sub>4</sub> cumulative production ( $\beta_1 = 1.43$ ,  $p$ -value =  $1.35 \times 10^{-3}$ ) (Table 3).

An interaction effect was found between the fractions of TiO<sub>2</sub> and ZnO used in the photocatalyst mixture with a statistically

significant ( $p$ -value =  $2.30 \times 10^{-2}$ ) and negative impact ( $\beta_3 = -2.64$ ) on CH<sub>4</sub> cumulative production (Table 3). This would indicate that the inclusion of ZnO significantly hampered the production of CH<sub>4</sub>.

These results were not encouraging from an activity point of view but they offered an opportunity for further scientific enquiry. Both TiO<sub>2</sub> and ZnO were synthesised using a precipitation method that employed sulphate salts TiOSO<sub>4</sub> and ZnSO<sub>4</sub>, respectively. Ion chromatography (IC) analyses were performed on pristine TiO<sub>2</sub> and ZnO samples, showing 0.4% and 12.0% wt sulphates, respectively. The large amount of sulphates observed in the ZnO samples, was also confirmed by XRD analysis (Fig. 7), showing that this material is actually composed of 43% Zn<sub>3</sub>O(SO<sub>4</sub>)<sub>2</sub>, corresponding to 20.7% wt amount of sulphates, and 57% ZnO.<sup>47</sup> The difference in the amount of sulphates recorded by IC and XRD is likely due to the inability of the IC analysis extraction procedure to recover all the sulphates. Sulphur and zinc mapped very closely to one another by SEM/EDX analysis (Fig. 8). Visually, sulphur content increased with increasing fraction of ZnO (Fig. 8). The EDX analysis also yielded a linear increase in sulphur with increasing the fraction of ZnO used (Fig. 9). Together, these were additional pieces of evidence highlighting the incorporation of sulphates by the ZnO used.

Lo *et al.* reported acidic sulphate modified titania as an efficient photocatalyst for CO<sub>2</sub> photoreduction<sup>48</sup> Nevertheless, sulphate anions was observed to have a detrimental effect on photooxidation by acting as both radical scavenger<sup>49</sup> and competing with reagents for adsorption to active photocatalyst sites.<sup>50</sup> We can discount the latter hypothesis since as discussed in Section 3.2.1, ZnO was observed to improved CO<sub>2</sub> adsorption. The radical (or hole) scavenging hypothesis was thus considered. Several mechanisms, all involving radical intermediates, have been proposed for CO<sub>2</sub> photoreduction.<sup>22,51</sup> Sulphates or species arising from radical scavenging yielding SO<sub>4</sub><sup>•-</sup> species

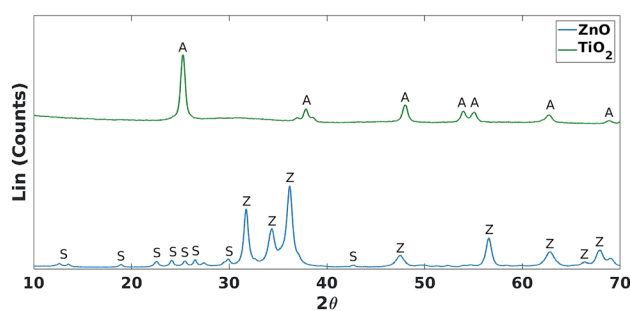


**Fig. 7** XRD comparison of TiO<sub>2</sub> and ZnO. A = anatase (TiO<sub>2</sub> phase), Z = zincite (ZnO phase) and S = Zn<sub>3</sub>O(SO<sub>4</sub>)<sub>2</sub>.

**Table 3** Coefficient values estimated for fitting model (2) and their respective  $p$ -values ( $*p$ -value  $< 0.05$ ) on CO and CH<sub>4</sub> cumulative production

Regression results for CO cumulative production			Regression results for CH <sub>4</sub> cumulative production		
Parameter coefficient	Value estimated	$p$ -Value	Parameter coefficient	Value estimated	$p$ -Value
$\beta_1$	9.71	$2.93 \times 10^{-4}$ *	$\beta_1$	1.43	$1.35 \times 10^{-3}$ *
$\beta_2$	1.96	$7.51 \times 10^{-2}$	$\beta_2$	0.12	$5.50 \times 10^{-1}$
$\beta_3$	0.53	$8.83 \times 10^{-1}$	$\beta_3$	-2.64	$2.30 \times 10^{-2}$ *



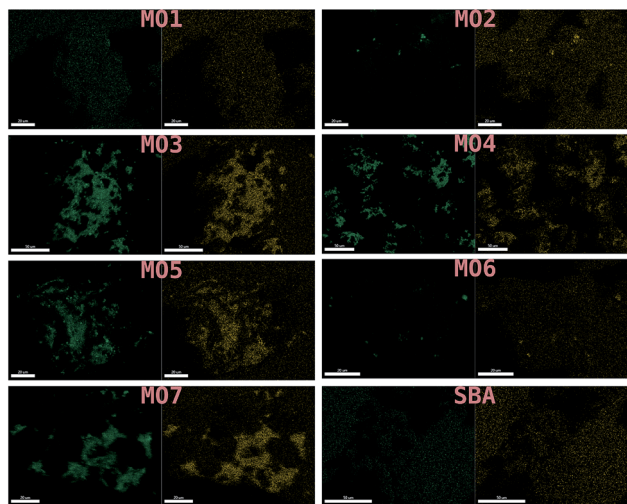


Fig. 8 SEM/EDX of MO1–MO7 and the SBA-15 support used. Zinc mapped on the left and sulphur on the right.

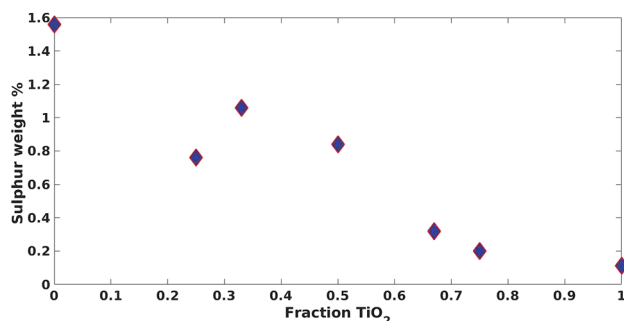


Fig. 9 Impact of increasing fraction of TiO<sub>2</sub> on approximated sulphur weight% from SEM/EDX.

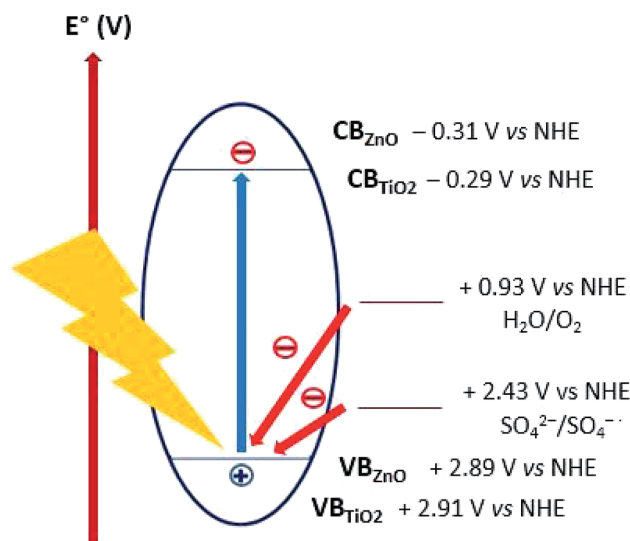


Fig. 10 Energy levels scheme for the proposed mechanism of sulphates as hole scavengers.

might interfere with the CO<sub>2</sub> photoreduction reaction pathway. Moreover, the oxidizing holes generated on both TiO<sub>2</sub> (+2.91 V vs. NHE) and ZnO (+2.89 V vs. NHE) valence band,<sup>18</sup> can be potentially scavenged by sulphates ( $E^\circ = +2.43$  V vs. NHE),<sup>52</sup> thus acting as charge carrier trap and competing with water oxidation (Fig. 10). The sulphates acting as radical and/or hole scavengers are very likely to undergo chemical transformations towards reduced sulphur species such as H<sub>2</sub>S, SO<sub>2</sub> and S. To confirm this hypothesis, future work would include attempting to identify these species formed during the CO<sub>2</sub> photoreduction reaction.

## 4 Conclusion

A systematic experimental mixture design as used to investigate the impact of the fractions of TiO<sub>2</sub> and ZnO as mixed MOs on an ordered SBA-15 mesoporous support for CO<sub>2</sub> photoreduction activity. The combination of a systematic experimental mixture design using numerical tools and the analysis of the prepared TiO<sub>2</sub>/ZnO photocatalyst properties offered an opportunity to provide evidence for the trapping of radical CO<sub>2</sub> photoreduction intermediates and/or charge carriers by sulphate groups. This approach has shown use for rapid screening and the development of mixed MOs for CO<sub>2</sub> photoreduction.

Increasing the fraction of ZnO increased the adsorption of CO<sub>2</sub> with statistical confirmation using the mixture design. Increasing the fraction of TiO<sub>2</sub> improved the production of CO with a linear trend observed. Increasing the fraction of TiO<sub>2</sub> also improved the production of CH<sub>4</sub> with an exponential trend observed. This was confirmed by numerical analysis where the fraction of TiO<sub>2</sub> was found to be statistically significant for both CO and CH<sub>4</sub> cumulative production. The exponential trend for CH<sub>4</sub> cumulative production could be explained by the statistical significance of a negative interaction between the fraction of TiO<sub>2</sub> and ZnO used. Increasing the fraction of ZnO yielded significantly less CH<sub>4</sub> production and had a slightly less dramatic, albeit still negative, impact on CO production.

The impact of radical scavengers on deactivation has not been explored for CO<sub>2</sub> photoreduction. The mixed MO mixtures was initially intended to improve the efficiency of CO<sub>2</sub> photoreduction. However, this study showed how the inclusion of sulphates from the synthesis method very likely led to deactivation and lower production of CH<sub>4</sub> and CO. In addition, this study serves as a framework for the efficient and systematic study of other novel photocatalyst synthetic techniques and subsequent formulation of novel mixtures for CO<sub>2</sub> photoreduction.

## Conflicts of interest

There are no conflicts to declare.

## Acknowledgements

The authors thank the financial support provided by the Engineering and Physical Sciences Research Council (EP/K021796/1), the Research Centre for Carbon Solutions (RCCS) and the James Watt Scholarship Programme at Heriot-Watt University.



We are also grateful for the support provided by the Buchan Chair in Sustainable Energy Engineering.

## Notes and references

- O. Ola and M. Maroto-Valer, *J. Photochem. Photobiol., C*, 2015, **24**, 16–42.
- A. Olivo, D. Zanardo, E. Ghedini, F. Menegazzo and M. Signoretto, *ChemEngineering*, 2018, **2**, 42.
- Y. Belmoujahid, M. Bonne, Y. Scudeller, D. Schleich, Y. Grohens and B. Lebeau, *Microporous Mesoporous Mater.*, 2015, **201**, 124–133.
- D. Zhao, Q. Huo, J. Feng, B. F. Chmelka and G. D. Stucky, *J. Am. Chem. Soc.*, 1998, **120**, 6024–6036.
- C. Zhao, L. Liu, Q. Zhang, J. Wang and Y. Li, *Catal. Sci. Technol.*, 2012, **2**, 2558–2568.
- R. Chen, X. Cheng, X. Zhu, Q. Liao, L. An, D. Ye, X. He and Z. Wang, *Chem. Eng. J.*, 2017, **316**, 911–918.
- C.-C. Yang, J. Vernimmen, V. Meynen, P. Cool and G. Mul, *J. Catal.*, 2011, **284**, 1–8.
- K. Li, B. Peng and T. Peng, *ACS Catal.*, 2016, **6**, 7485–7527.
- X. Chang, T. Wang and J. Gong, *Energy Environ. Sci.*, 2016, **9**, 2177–2196.
- X. Liu, L. Ye, S. Liu, Y. Li and X. Ji, *Sci. Rep.*, 2016, **6**, 38474.
- W.-N. Wang, F. Wu, Y. Myung, D. M. Niedzwiedzki, H. S. Im, J. Park, P. Banerjee and P. Biswas, *ACS Appl. Mater. Interfaces*, 2015, **7**, 5685–5692.
- C. Xin, M. Hu, K. Wang and X. Wang, *Langmuir*, 2017, **33**, 6667–6676.
- Y. Li, W. Xie, X. Hu, G. Shen, X. Zhou, Y. Xiang, X. Zhao and P. Fang, *Langmuir*, 2010, **26**, 591–597.
- X. Zhang, J. Qin, Y. Xue, P. Yu, B. Zhang, L. Wang and R. Liu, *Sci. Rep.*, 2014, **4**, 4596.
- S. Krischok, O. Höfft and V. Kempter, *Surf. Sci.*, 2002, **507–510**, 69–73.
- M. Quintana, T. Edvinsson, A. Hagfeldt and G. Boschloo, *J. Phys. Chem. C*, 2007, **111**, 1035–1041.
- H. Li, D. Gao, P. Gao, F. Wang, N. Zhao, F. Xiao, W. Wei and Y. Sun, *Catal. Sci. Technol.*, 2013, **3**, 2801–2809.
- G. Xi, S. Ouyang and J. Ye, *Chem.–Eur. J.*, 2019, **17**, 9057–9061.
- K. Wu, X. Dong, J. Zhu, P. Wu, C. Liu, Y. Wang, J. Wu, J. Hou, Z. Liu and X. Guo, *J. Mater. Sci.*, 2018, **53**, 11595–11606.
- V. Sukharev and R. Kershaw, *J. Photochem. Photobiol., A*, 1996, **98**, 165–169.
- N. Serpone, P. Maruthamuthu, P. Pichat, E. Pelizzetti and H. Hidaka, *J. Photochem. Photobiol., A*, 1995, **85**, 247–255.
- F. Fresno, I. J. Villar-García, L. Collado, E. Alfonso-González, P. Reñones, M. Barawi and V. A. de la Peña O'Shea, *J. Phys. Chem. Lett.*, 2018, **9**, 7192–7204.
- L. Liu, C. Zhao, D. Pitts, H. Zhao and Y. Li, *Catal. Sci. Technol.*, 2014, **4**, 1539–1546.
- W. N. Wang, W. J. An, B. Ramalingam, S. Mukherjee, D. M. Niedzwiedzki, S. Gangopadhyay and P. Biswas, *J. Am. Chem. Soc.*, 2012, **134**, 11276–11281.
- S. Poudyal and S. Laursen, *J. Phys. Chem. C*, 2018, **122**, 8045–8057.
- P. Reñones, A. Moya, F. Fresno, L. Collado, J. J. Vilatela and V. A. de la Peña O'Shea, *J. CO<sub>2</sub> Util.*, 2016, **15**, 24–31.
- L. Liu, C. Zhao, J. T. Miller and Y. Li, *J. Phys. Chem. C*, 2017, **121**, 490–499.
- Y. Li, W.-N. Wang, Z. Zhan, M.-H. Woo, C.-Y. Wu and P. Biswas, *Appl. Catal., B*, 2010, **100**, 386–392.
- W. A. Thompson, C. Perier and M. M. Maroto-Valer, *Appl. Catal., B*, 2018, **238**, 136–146.
- F. Fresno, P. Reñones, E. Alfonso, C. Guillén, J. F. Trigo, J. Herrero, L. Collado and V. A. de la Peña O'Shea, *Appl. Catal., B*, 2018, **224**, 912–918.
- L. Liu, F. Gao, H. Zhao and Y. Li, *Appl. Catal., B*, 2013, **134–135**, 349–358.
- H. Zhao, L. Liu, J. M. Andino and Y. Li, *J. Mater. Chem. A*, 2013, **1**, 8209–8216.
- L. Gomathi Devi, S. Girish Kumar, K. Mohan Reddy and C. Munikrishnappa, *J. Hazard. Mater.*, 2009, **164**, 459–467.
- M. Chiha, O. Hamdaoui, S. Baup and N. Gondrexon, *Ultrason. Sonochem.*, 2011, **18**, 943–950.
- F. Häse, L. M. Roch and A. Aspuru-Guzik, *Trends Chem.*, 2019, **1**, 282–291.
- J. Antony, *Design of Experiments for Engineers and Scientists*, Elsevier Science, 2014.
- L. Ilzarbe, M. J. Álvarez, E. Viles and M. Tanco, *Qual. Reliab. Eng. Int.*, 2019, **24**, 417–428.
- C. C. Solvason, N. G. Chemmangattuvalappil, F. T. Eljack and M. R. Eden, *Ind. Eng. Chem. Res.*, 2009, **48**, 2245–2256.
- A. Olivo, E. Ghedini, M. Signoretto, M. Compagnoni and I. Rossetti, *Energies*, 2017, **10**, 1394.
- E. Ghedini, M. Signoretto, F. Pinna and G. Cruciani, *Catal. Lett.*, 2008, **125**, 359–370.
- A. Olivo, V. Trevisan, E. Ghedini, F. Pinna, C. Bianchi, A. Naldoni, G. Cruciani and M. Signoretto, *J. CO<sub>2</sub> Util.*, 2015, **12**, 86–94.
- A. Escobedo-Morales, I. I. Ruiz-López, M. Ruiz-Peralta, L. Tepech-Carrillo, M. Sánchez-Cantú and J. E. Moreno-Orea, *Heliyon*, 2019, **5**, e01505.
- S. Brunauer, P. H. Emmett and E. Teller, *J. Am. Chem. Soc.*, 1938, **60**, 309–319.
- C. Sarzanini, G. Sacchero, F. Pinna, M. Signoretto, G. Cerrato and C. Morterra, *J. Mater. Chem.*, 1995, **5**, 353–360.
- W. Liu and Y. Zhang, *J. Mater. Chem. A*, 2014, **2**, 10244–10249.
- M. M. Demir, R. Muñoz-Espí, I. Lieberwirth and G. Wegner, *J. Mater. Chem.*, 2006, **16**, 2940–2947.
- A. Moezzi, M. B. Cortie and A. M. McDonagh, *Dalton Trans.*, 2013, **42**, 14432–14437.
- C.-C. C. Lo, C.-H. H. Hung, C.-S. S. Yuan and Y.-L. L. Hung, *Chin. J. Catal.*, 2007, **28**, 528–534.
- W. Zhang, T. An, M. Cui, G. Sheng and J. Fu, *J. Chem. Technol. Biotechnol.*, 2004, **80**, 223–229.
- P.-S. Yap and T.-T. Lim, *Appl. Catal., B*, 2011, **101**, 709–717.
- S. N. Habisreutinger, L. Schmidt-Mende and J. K. Stolarczyk, *Angew. Chem., Int. Ed.*, 2013, **52**, 7372–7408.
- R. E. Huie, C. L. Clifton and P. Neta, *Int. J. Radiat. Appl. Instrum., Part C*, 1991, **38**, 477–481.

